Ordering of anisotropic nanoparticles in diblock copolymer lamellae: Simulations with dissipative particle dynamics and a molecular theory

Anatoly V. Berezkin[1], Yaroslav V. Kudryavtsev[2,3,a)], Maxim V. Gorkunov[4] and Mikhail A. Osipov[2,5]

[1] *Technische Universität München,*

James-Franck-Str. 1, 85747 Garching, Germany

[2] *Topchiev Institute of Petrochemical Synthesis, Russian Academy of Sciences,*

Leninsky prosp. 29, 119991 Moscow, Russia

[3] *Frumkin Institute of Physical Chemistry and Electrochemistry,*

Russian Academy of Sciences, Leninsky prosp. 31, 119071 Moscow, Russia

[4] *Shubnikov Institute of Crystallography, Federal Scientific Research Centre*

"Crystallography and Photonics", Russian Academy of Sciences,

Leninsky prosp. 59, 119333 Moscow, Russia

[5] *Department of Mathematics, University of Strathclyde, Glasgow G1 1XH, Scotland, UK*

Short title: Ordering of anisotropic nanoparticles: Simulations and theory

[a)] Corresponding author. Electronic mail: yar@ips.ac.ru

ABSTRACT

Local distribution and orientation of anisotropic nanoparticles in microphase-separated symmetric diblock copolymers has been simulated using dissipative particle dynamics and analyzed with a molecular theory. It has been demonstrated that nanoparticles are characterized by a non-trivial orientational ordering in the lamellar phase due to their anisotropic interactions with isotropic monomer units. In the simulations, the maximum concentration and degree of ordering are attained for non-selective nanorods near the domain boundary. In this case the nanorods have a certain tendency to align parallel to the interface in the boundary region and perpendicular to it inside the domains. Similar orientation ordering of ~~spherical~~ nanoparticles located at the lamellar interface is predicted by the molecular theory which takes into account that the nanoparticles interact with monomer units via both isotropic and anisotropic potentials. Computer simulations enable one to study the effects of the nanorod concentration, length, stiffness, and selectivity of their interactions with the copolymer components on the phase stability and orientational order of nanoparticles. If the volume fraction of the nanorods is lower than 0.1, they have no effect on the copolymer transition from the disordered state into a lamellar microstructure. Increasing nanorod concentration or nanorod length results in clustering of the nanorods and eventually leads to a macrophase separation, whereas the copolymer preserves its lamellar morphology. Segregated nanorods of length close to the width of the diblock copolymer domains are stacked side by side into smectic layers that fill domain space. Thus, spontaneous organization and orientation of nanorods leads to a spatial modulation of anisotropic composite properties ~~creating an opportunity to align block copolymers by external fields~~ which may be important for various applications.

KEYWORDS: diblock copolymer, nanoparticles, dissipative particle dynamics, molecular theory, phase separation, microstructure, anisotropy, orientational order

I. INTRODUCTION

After a sixty-year history of block copolymer studies the macromolecules composed of long chemically different monomer unit sequences have become well-defined objects capable of exhibiting nanostructures with diverse morphology and periodicity.[1] Various methods for the directed self-assembly of thin block copolymer films have been developed almost up to the technological level.[2,3] Although the potential of pure block copolymers in the design of lithography,[4] photovoltaic,[5] membrane,[6] and other functional materials is not fully realized yet,[7] there is a significant evidence that it can be further multiplied in hybrid composites with nanoparticles[8-10] that are able to form highly-organized structures via self-organisation.[11] Depending on their chemical nature, nanoparticles can in `fact considerably improve mechanical, barrier, electric, optical, and other characteristics of matrix polymers while preserving their good processability.[12,13] However, the design of such composite systems usually requires a sophisticated strategy that encompasses nanoparticle synthesis, surface modification, directed introduction into the polymer bulk, and stabilization there. In the block copolymer case the problem is only complicated by the selectivity of nanoparticles towards different blocks and local perturbations that they introduce into the copolymer microstructure. As a result, the directed self-assembly of block copolymer films in the presence of nanoparticles is still limited to rare laboratory experiments.[14,15]

Among many factors that determine the complex behavior of hybrid composites, the anisotropy of the nanofillers is one of the most important properties. It affects the total system anisotropy, which is a target parameter in charge and molecular transport, light conversion, and other functional applications. Whereas this is indisputable for 2D nanostructures[13] (clay platelets, graphene sheets) and 1D nanostructures with high (>10) aspect ratio[16-21] (nanowires, nanotubes), the anisotropy of nanoparticles has so far received limited attention in spite of their shape abundance offered by synthetic chemistry.[22,23] Perhaps the simplest small anisotropic objects are nanorods, and their behavior in block copolymer films has been considered in Refs. 24-36, which are mainly short communications just focused into the visualization of the morphology of the prepared composites. In any case the number of

publications dealing with anisotropic nanoparticles in block copolymers is vanishingly small compared with the total number of publications on block copolymer nanocomposites over the past decade.

In the existing studies, the host matrices are limited to the diblock copolymers of PS with PMMA,[24,27-31] P2VP,[26,36] and modified P4VP,[25,32-35] doped with nanorods made of Au,[24-26] ZnO,[27] CdSe,[28-34] CuPt,[35] and Fe_2P[36] and covered by low- or high-molecular mass ligands providing their selective localization in a particular block copolymer domain. At the present stage, controlling such a selectivity and preventing nanorod aggregation are considered to be the main results. Other observations include preferential alignment of nanorods along lamellar or cylindrical domain walls or micelles,[24,25,27,28,31-36] alignment in the direction perpendicular to the boundaries,[25,29,30] segregation of nanorods at the substrate[24,26] or at the free surface,[29-31] and changes in the domain morphology and orientation.[31,34] In general, the reported results are mainly qualitative and the information on the role of nanorod concentration, size, aspect ratio, and ligand structure of the surface layer is rather fragmentary.

Theoretical research on polymer-based nanocomposites is also at its early stage. Phase behavior of pure block copolymers is effectively captured by the field-theoretic approaches,[37] including in particular the self-consistent field theory (SCFT).[38] In the case of polymer nanocomposites the distribution of nanoparticles can be accounted for by combining SCFT with the density functional theory.[39,40] On the other hand, the accuracy of field-based techniques in describing the orientation of the anisotropic particles and, therefore, in predicting the macroscopic anisotropy of the composite is quite limited. As an alternative, hybrid particle-field approaches have been developed[41-43] that employ particle-to-field transformation for polymer chains but retain explicit treatment of nanoparticles. Formally such an approach enables one to consider nanoparticles of arbitrary shape and even grafted with polymers but at the same time it increases the computational cost and causes inherent difficulties in the simultaneous solution of partial differential equations and implementation of simulation procedures.[44] As a result, the number of publications on the topic is still very limited.[26,45]

A possible simplification here is to fix the phase-separated structure of a diblock copolymer in order to study in detail the spatial distribution and orientational ordering of anisotropic nanoparticles in

such a system. This can be a promising reasonable approach. On the one hand, the volume fraction of nanoparticles in polymer composites is usually low (< 0.1) and, therefore, it is not expected, at least thermodynamically, to considerably affect the copolymer morphology. On the other side, the model of composite where the nanorods are subject to a given molecular field has a clear liquid-crystalline motif and hence the corresponding theoretical results can be used. Recently, two of us have developed a molecular mean-field theory which enables one to describe the spatial distribution and nematic ordering of anisotropic nanoparticles in lamellae and hexagonal phases of block copolymers.[46] In that model a nanoparticle is treated as a spherical object possessing some anisotropic properties and interacting with monomer units of polymer chains via a potential composed of isotropic and anisotropic parts. Whereas the isotropic interaction determines the location of nanoparticles depending on their selectivity with respect to chemically different monomer units, the anisotropic interaction (which apparently has not been introduced before in the theory of polymer nanocomposites) is responsible for the nanoparticle ordering and alignment relative to the copolymer domains. The most interesting effect predicted in Ref. 46 is the possibility of mutually perpendicular preferential orientation of anisotropic nanoparticles in neighboring domains.

In this study, we perform a coarse-grained molecular dynamics simulation of nanorods distribution and alignment in the lamellar block copolymer microstructure. Using dissipative particle dynamics (DPD) we locate the order-disorder transition in the composite, describe the stationary spatial distribution of its components, and investigate the role of nanorod content, length, stiffness, and selectivity. Large-scale molecular simulations of nanoparticle self-assembly in polymeric systems still remain a challenge[47] and DPD is currently the only reported technique to study the effect of monodisperse,[48,49] bidisperse,[50] and diblock (Janus-like)[51] nanorods on the diblock copolymer lamellar[48,50,51] and hexagonal[49-51] phases and the behavior of carbon nanotubes (modeled as large nanorods) in concentrated diblock copolymer solutions.[52] Ref. 48 can be called a predecessor of the present study carried out in a much smaller (ten times by volume) simulation box and focused on the morphological changes introduced by adding more and more nanorods rather than on the local

distribution of the composite components and orientational order of the nanorods, which is the primary aim of this study. For example, the orientational (nematic) order parameter reported in Ref. 48 is an average over the entire system, whereas we evaluate it locally and study the corresponding order parameter profiles in different domains.

The paper is arranged as follows. In the next section we describe the simulation method and algorithms used for the data processing. Then we present and discuss the simulation results. A special section contains a summary of the theory proposed in Ref. 46 and the numerical results of the theory are compared with the results of computer simulations. Finally, we consider the prospects for observing the predicted effects in laboratory experiments and summarize our findings.

II. SIMULATION MODEL

A. Dissipative particle dynamics

In this study, we use dissipative particle dynamics (DPD), a well-known coarse-grained molecular dynamics technique proposed by Hoogerbrugge and Koelman[53,54] for the simulation of liquid suspensions and extended to polymer systems by Espanol, Groot and Warren[55,56] by mapping it onto the classical Flory-Huggins theory.

DPD particles, each representing a group of repeating units constituting a polymer chain, interact by conservative, dissipative, and random forces, which are pairwise additive. The net force $\mathbf{f}_i = \sum_{j \neq i} (\mathbf{F}_{ij}^C + \mathbf{F}_{ij}^D + \mathbf{F}_{ij}^R)$ acting on a given particle i is calculated by summation over all other particles within a certain cut-off radius r_c. Let r_c, the particle mass, m, and $k_B T$ be the unit distance, mass, and thermal energy, respectively, thus defining the unit time $\tau_0 = r_c \sqrt{m / k_B T}$.

The conservative force represents the excluded volume interactions and elastic interactions of particles i and j in the dimensionless form $\mathbf{F}_{ij}^C = a_{ij}(1 - r_{ij})\hat{\mathbf{r}}_{ij} - k_s \mathbf{r}_{ij}$, where $\mathbf{r}_{ij} = \mathbf{r}_i - \mathbf{r}_j$, $r_{ij} = |\mathbf{r}_{ij}|$, $\hat{\mathbf{r}}_{ij} = \mathbf{r}_{ij} / r_{ij}$; a_{ij} is a maximum repulsion between those particles attained at $\mathbf{r}_i = \mathbf{r}_j$; and k_s is a Hookean spring constant, which is taken to be $k_s = 4$ for particles linked in a polymer chain and zero for non-

bonded particles. The dissipative and random forces, $\mathbf{F}_{ij}^{D} = -\gamma\omega(r_{ij})^2(\hat{\mathbf{r}}_{ij}\cdot\mathbf{v}_{ij})\hat{\mathbf{r}}_{ij}$ and $\mathbf{F}_{ij}^{R} = \sigma\omega(r_{ij})\hat{\mathbf{r}}_{ij}\zeta/\sqrt{\delta t}$, respectively, constitute the Groot-Warren thermostat,[56] where γ is a friction coefficient related to a thermal noise amplitude σ via the fluctuation-dissipation theorem, $\sigma^2 = 2\gamma;\omega(r)$ is a weight function, ζ is a normally distributed random variable with zero mean and unit variance, which is uncorrelated for different particle pairs, δt is the time step of an integration scheme, and $\mathbf{v}_{ij} = \mathbf{v}_i - \mathbf{v}_j$ is the relative velocity of particles i and j. Following Ref. 56, we choose $\sigma = 3$, $\omega(r) = 1 - r$, and the average density of particles $\rho_0 = 3$.

The simulation box of sizes $l_x \times l_y \times l_z = 24 \times 24 \times 24\ r_c^3$ periodic in all three directions is used. It is filled with a total of 41472 DPD particles of three kinds, A, B, and R. A diblock copolymer chain $A_{10}B_{10}$ consists of $N = 20$ bonded particles forming A and B blocks of $N_A = N_B = 10$. The chains are thermostated as described above. All nanorods are made of $N_R = 3$, 4, 5, or 7 R particles connected by rigid bonds of the constant length $b_R = 0.7r_c$. Spring-like bond potentials do not apply in this case. Nanorods are simulated as rigid bodies in the NVE ensemble using an algorithm by Miller et al.[57] Their correct temperature is maintained through the interactions with the thermostated polymeric DPD liquid surrounding them. It is worth noting that semi-rigid mesogens can be also simulated with DPD using an additional spring force between their first and last particles[58] or by introducing angle potentials.[59] For the sake of comparison we perform some simulations by replacing nanorods with flexible chains consisting of $N_R = 5$ particles of R type.

The equations of particle motion, $d\mathbf{r}_i / dt = \mathbf{v}_i$, $d\mathbf{v}_i / dt = \mathbf{F}_i$, are solved numerically using a free source code LAMMPS[60] that implements the so called DPD-VV integration scheme[61] (modified velocity-Verlet algorithm) with a time step $\delta t = 0.02$.

In Ref. 56 it was recommended to use the repulsion parameter between similar particles of a DPD liquid, $a_{\alpha\alpha} = 25$, in order to match the compressibility of water at the chosen particle density $\rho_0 = 3$. However, our preliminary simulations of a pure nanorod melt with $N_R = 5$, $k_BT = 1$, and $a_{RR} = 25$

demonstrated no ordering (Fig. 1, left picture) due to weak excluded-volume interactions. This agrees with the literature, where it is reported that rigid[62] and semi-rigid[63] rods reveal a noticeable order at $N_R \geq 7$ and $k_BT \leq 0.7$. It means that for the composite modeling we would have to consider only nanorods which length exceeds the period of a lamellar structure in diblock copolymers. Then, it is inconvenient to vary the temperature in a DPD model since it simultaneously affects both repulsive forces and thermal fluctuations.

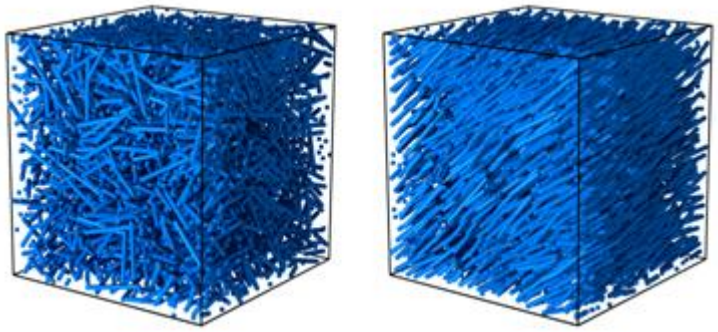

FIG. 1. Ordering in a melt of nanorods with $N_R = 5$ upon increasing the repulsion parameter a_{RR} from 25 (left) to 50 (right).

The tendency to order can also be enhanced by adding a soft attractive anisotropic potential to the particles constituting neighboring nanorods.[63] In this paper we use another method to achieve the same goal by increasing the repulsion parameter $a_{\alpha\alpha}$ (α = A, B, or R) from the value of 25 up to 50 for similar particles, thus giving no importance to a particular value of the DPD liquid compressibility. This appears to be sufficient for achieve the nematic ordering in the melt of nanorods with $N_R = 5$ at $k_BT = 1$ (Fig. 1, right) and we anticipate a similar ordering in their composite with the copolymer matrix.

The interaction of nanorod particles with A and B blocks is described by a selectivity parameter $\sigma = (a_{RB} - a_{RA})/(a_{AB} - a_{RA})$, which varies from zero for the non-selective case, when $a_{RB} = a_{RA} = 50$, to unity for the highest selectivity, when A and R particles are the same so that $a_{RB} = a_{AB}$. The overall

volume fraction of nanorods in the majority of simulations takes the values ϕ_R = 0, 0.01, 0.02, 0.05, and 0.1, while the net volume fractions of A and B units are equal to $\phi_A = \phi_B = (1 - \phi_R)/2$.

B. Simulation data processing

DPD simulations enable us to visualize stationary states of the composite and to describe them in terms of the local volume fractions of A, B, and R particles, $\phi_A(\mathbf{r})$, $\phi_B(\mathbf{r})$, and $\phi_R(\mathbf{r})$, and the scalar orientational order parameter, $S(\mathbf{r})$, that characterizes the average orientation of nanorod axes $\boldsymbol{a}$ ($|\boldsymbol{a}| = 1$) relatively to the unit normal to lamellar planes, $\mathbf{h}$:

$$S(\mathbf{r}) = \left\langle \frac{1}{2}\left[3(\boldsymbol{a}(\mathbf{r})\cdot\mathbf{h})^2 - 1\right]\right\rangle, \qquad (1)$$

where the angular brackets denote the averaging over a local subset of rods. Zero value of the order parameter corresponds to an uncorrelated orientation of nanorods, whereas $S > 0$ ($S < 0$) indicates their tendency to perpendicular (parallel) orientation with respect to the lamellar plane. In general, $-0.5 \le S \le 1$.

When a lamellar microstructure is formed, we are interested in the distribution of all components along the normal to the layers. However, the orientation of lamellas in a periodic simulation box is random and a regular procedure for extracting the desired distribution is needed. We make use of the fact that a normal to the lamellar plane can be defined as an average vector connecting the centers of masses of blocks A and B in one copolymer chain. Such connecting vectors are plotted for all copolymers in the system, then normalized to the unit length and translated so that their starting points coincide. Ends of those vectors now form a cloud of 10^5 points $\mathbf{p}_i = \{p_{i,x}, p_{i,y}, p_{i,z}\}$ non-uniformly distributed over the surface of a unit sphere. The gyration tensor of this cloud is defined as

$$J = \begin{Vmatrix} J_{xx} & J_{xy} & J_{xz} \\ J_{yx} & J_{yy} & J_{yz} \\ J_{zx} & J_{zy} & J_{zz} \end{Vmatrix}, \qquad J_{\alpha\beta} = \frac{1}{n}\sum_{i=1}^{n} p_{i,\alpha}\, p_{i,\beta}\ . \qquad (2)$$

Diagonalization of J yields three eigenvalues and the three corresponding eigenvectors. The eigenvector corresponding to the largest eigenvalue is the desired vector **h**, which is normal to the lamellar planes. In what follows, we designate its direction as the z-axis. All local variables describing the composite structure are expressed as the functions of z: $\phi_A(z)$, $\phi_B(z)$, $\phi_R(z)$, $S(z)$, while the center of a B layer is chosen as the origin ($z = 0$).

III. RESULTS AND DISCUSSION

A. Order-disorder transition

Microphase separation in the pure diblock copolymer $A_{10}B_{10}$ and its composites with nanorods has been simulated by annealing the initially disordered structures upon a gradual, incremental (by 0.1) increase in the repulsion parameter between dissimilar DPD particles, a_{AB}. An order-disorder transition (ODT) has been identified by a drop in the potential energy of the ordered system (Fig. 2), appearance of a secondary peak in the static structure factor (the primary peak was shifted to $q \neq 0$ even in the disordered phase due to composition fluctuations) and visually from the structure snapshots (see Ref. 64 for the details).

A tendency of diblock copolymer to microphase separation is governed by the difference $\Delta a = a_{AB} - a_{AA}$, which is proportional to the Flory-Huggins interaction parameter:[56] $\chi = (0.306 \pm 0.003)\Delta a$. It has been found that in the pure copolymer melt with $a_{AA} = a_{BB} = 50$ the order-disorder transition (ODT) occurs at $a_{AB} = 55.7$ which corresponds to $\chi N = 34.9$.

One notes that the above-mentioned χ does not coincide with the effective parameter χ_e which enters the mean-field theory of Leibler.[65] The theory predicts phase separation in a melt of infinitely long ($N \to \infty$) diblock copolymer chains if the product $\chi_e N$ exceeds the critical value of 10.5. Extension of the Leibler's theory to finite N still constitutes a problem. Whereas fluctuation corrections calculated by Fredrickson and Helfand[66] in terms of the so-called invariant polymerization degree N_{inv} appear to be useful for interpretation of the experimental data, they can hardly be used in a quantitative

interpretation of the simulations that deal with relatively short chains. For instance, both DPD[67,68] and Monte Carlo[69] simulations of block copolymers typically yield critical values of χN which are considerably higher than 10.5. Only recently it has been shown[70-72] that the thermodynamics of any diblock copolymer melt is fully controlled by $\chi_e N$ and N_{inv}, while the relation between χ_e and the parameters $a_{\alpha\beta}$, which describe binary interactions between copolymer units, is nonlinear. A method to derive such a relationship has been suggested[70-72] based on the analysis of the simulated or the experimental static structure factor in terms of the fluctuation theory. Whereas this task is beyond our study, we can evaluate the critical value of $\chi_e N$ using the explicit formulae proposed in Ref. 70: $\chi_{cr}N = 10.5 + 41.0\, N_{inv}^{-1/3} + 123.0\, N_{inv}^{-0.56}$, where, by definition, $N_{inv} = N(\rho_0 b^3)^2$ is proportional to the number of polymer chains within the volume occupied by a given chain of N units. In our system $N = 20$, $\rho_0 = 3$, $b = 0.9037 r_c$ so that $N_{inv} = 98.0$ and hence the ODT occurs at $\chi_{cr}N = 28.8$. Here the parameter b has been calculated from a separate simulation of the homopolymer DPD liquid at $a = 50$ in a larger $32\times32\times32\ r_c^3$ box. It has been found that for $N > 100$ the gyration radius of a chain as a function of its polymerization degree, $R_g(N)$, is given asymptotically by the equation $R_g^2 = (0.13611 \pm 0.00001) N r_c^2$ from which $b^2 = \lim_{N\to\infty}(6R_g^2(N)/N)$ has been calculated. At the same time, substitution of the critical repulsion parameter $a_{\mathrm{AB}} = 55.7$ into the standard DPD relation $\chi = 0.306\Delta a$ yields $\chi_{cr}N = 34.9$, which means that this relation is incorrect at least outside the interval $2 \le N \le 10$ where it has originally been proposed in Ref. 56.

Potential energy of the composite, calculated from the simulation data, is presented in Fig. 2. One can readily see that the introduction of nanorods into the block copolymer melt does not have a pronounced effect on the critical value of the repulsion parameter a_{AB}, which falls into the range between 55.7 and 56.5, when the fraction of nanorods ϕ_{R} is increased from 0 to 0.1. The observed minor increase in the critical value of a_{AB} could be caused by screening of the interactions between A and B

blocks by the R particles. For ϕ_R = 0.2 the lamellae are heavily distorted and the potential energy is roughly monotonic in Fig. 2, while the ODT can still be detected visually.

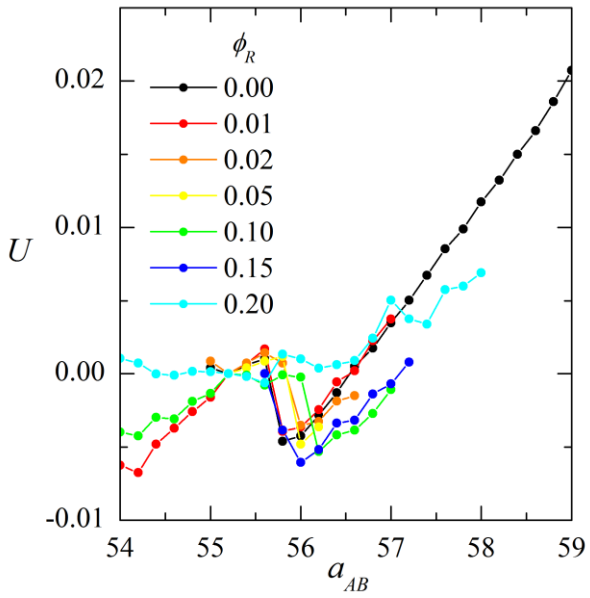

FIG. 2. Potential energy of the composite as a function of the repulsion parameter between A and B particles, a_{AB}, for different values of the average volume fraction of highly selective (σ = 1) nanorods, ϕ_R.

B. Local composite structure

For a symmetric copolymer the increase of the repulsion parameter a_{AB} above the ODT value leads to the formation of a lamellar microstructure. In the absence of a simple accurate relation between χ_e and $a_{\alpha\beta}$ we can use a crude equation

$$\frac{\chi_e N}{10.5} = \frac{\Delta a}{\Delta a_{cr}}, \qquad (3)$$

to estimate $\chi_e N$. One concludes that for $\Delta a = a_{AB} - a_{AA} = 20$ and $\Delta a_{cr} = 55.7 - 50 = 5.7$ our simulations correspond to $\chi_e N = 36.8$ for infinitely long chains, which is within the strong segregation regime. All simulations of microphase-separated composites described below have been carried out for $a_{AB} = 70$ when a well-defined structure with almost perfect domains is formed.

One expects that sufficiently anisotropic nanoparticles will be orientationally ordered in the polymer matrix or in their own phase. The corresponding structure snapshots are shown in Fig. 3 for the most selective case $\sigma = 1$, when the majority of the nanorods are located within A layers. One can readily see that the lamellar microstructure is preserved even at a high nanorod content, ϕ_R. Some distortions appear at $\phi_R > 0.1$ but no sign of a transition into the hexagonal or the bicontinuous morphology, predicted in Ref. 48, can be detected. We can merely assume that these transitions are the artifacts stemming from the small sizes of the simulation boxes which are comparable to the microstructure period.

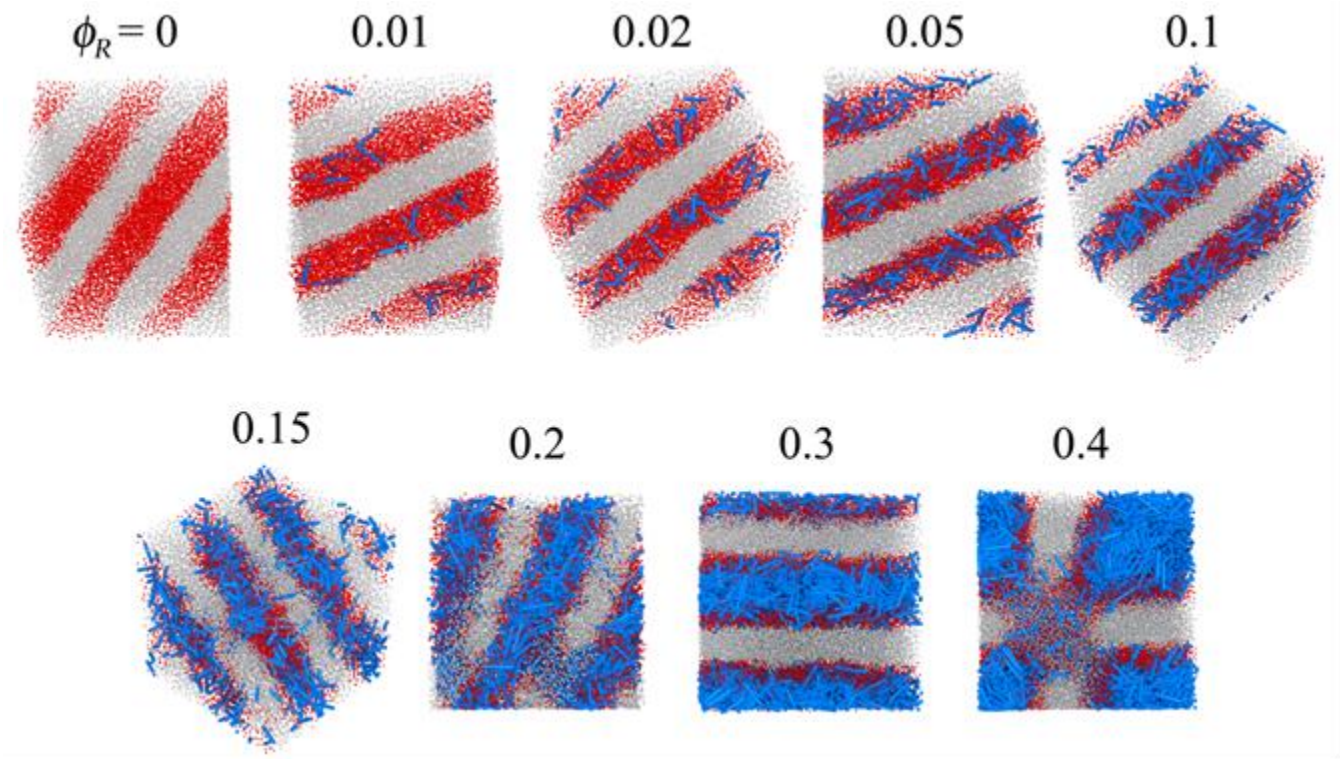

FIG. 3. Microphase-separated composites based on the diblock copolymer $A_{10}B_{10}$ doped with highly selective ($\sigma = 1$) nanorods (blue) with $N_R = 5$ for different values of the nanorod volume fraction, ϕ_R, specified above each snapshot. The monomer units A and B are shown in red and light grey, respectively.

Spatial profiles of the variables $\phi_A(z)$, $\phi_B(z)$, $\phi_R(z)$, and $S(z)$, which describe the local composite structure, are presented in Fig. 4 for several nanorod content values which are equal or higher then those used in Fig. 3. The z-axis is perpendicular to the lamellae and is scaled by the structure period d, which takes the values from 7.95 to $8.29r_c$ depending on the system composition. The model systems are strongly segregated, since there are no A units deeply inside B domains and vice versa. With $a_{RB} = a_{AB} = 70 > a_{RA} = a_{AA} = a_{BB} = a_{RR} = 50$, the nanorods are selectively located in the A domains with a maximum at the center and nearly linear concentration decay towards the boundaries.

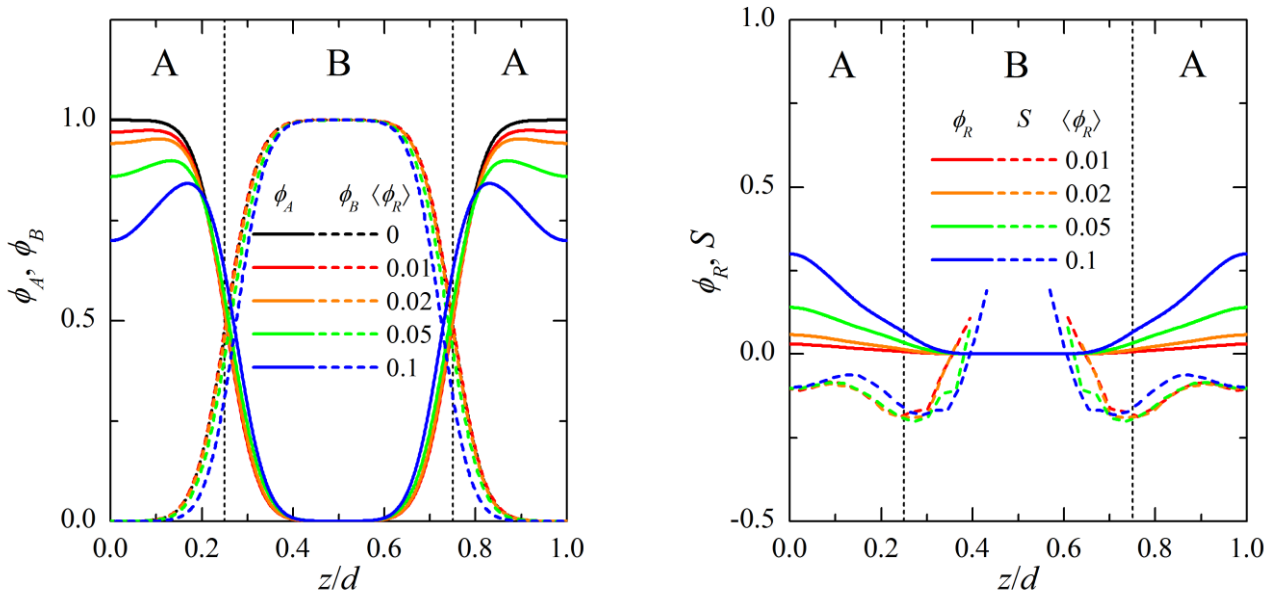

FIG. 4. The local volume fractions, $\phi_A(z)$ and $\phi_B(z)$, of the A and B particles (left), and the local volume fraction of the nanorods, $\phi_R(z)$, together with the orientational order parameter, $S(z)$, for different values of the average volume fraction of nanorods, ϕ_R, (right). In the interval $0.4 < z/d < 0.6$ the values of $S(z)$ are not shown because in this region the local nanorod content is very low giving rise to strong fluctuations. Vertical dashed lines show the domain boundaries in the pure diblock copolymer melt. In all cases $a_{AB} = 70$, $\sigma = 1$, and $N_R = 5$.

At $\phi_R < 0.1$ the local orientational order parameter S is only slightly dependent on the total concentration of nanorods, which indicates that their anisotropic interaction is weak. The order

parameter is negative in A domains thus indicating that nanorods prefer to align in the lamellar plane in order to avoid protruding their ends beyond the domain boundaries. Tilted nanorods are most easily pushed out of B domains and, therefore, the minimum of $S(z)$ is achieved at the A/B interface. The concentration of nanorods in the bulk of B domains is very low but those few that are located there are aligned across the lamella, because in that case their ends have a chance to reach neighboring A domains (note that the nanorod length $(N_R - 1)b_R = 2.8r_c$ is nearly 2/3 of the domain width). Accordingly, $S(z)$ is positive at the center of B domains though exact values are inaccessible because of the strong concentration fluctuations in those sparsely populated ($\phi_R(z = 0) << 1$) regions. Simulations of composites with slightly less selective nanorods have shown that $S(z)$ indeed achieves a maximum at $z = 0$. The composite with $\phi_R = 0.1$ is characterized by a non-monotonic behavior of $S(z)$ and by the undulations of the $\phi_R(z)$ profiles within A domains (Fig. 4), which possibly reflect the effects of nanorod interactions.

C. Effects of the nanorod length and stiffness

Snapshots of the ordered diblock copolymers $A_{10}B_{10}$ doped by highly selective ($\sigma = 1$) nanorods consisting of 3, 4, and 5 spherical particles are shown in Fig. 5 for $\phi_R = 0.1$. Visually all the systems are similar except for some clustering of longer nanorods. The corresponding local composition and orientational order parameter profiles are shown in Fig. 6 for the same composites, including the system containing flexible chains with $N_R = 5$ instead of nanorods. It can be seen that the nanorod length and stiffness have almost no effect on the local composition, which appears to be mainly defined by the repulsion between dissimilar DPD particles. Orientation of nanorods is slightly more affected: whereas nanorods with $N_R = 5$ demonstrate certain alignment in the direction of A-domain axis, the absolute value of the orientational order parameter naturally decreases with the decreasing nanorod length and completely vanishes for the flexible filler.

The system with nanorods concentrated in one of the copolymer blocks seems to be the only one, which has been implemented so far in the laboratory experiments.[24-36] Alignment of nanorods along the

domain axes, predicted by our simulations, is achieved when the excessive nanorod aggregation is suppressed by imposing geometrical constraints in narrow domains[24,27,28,31,36] or using specific pre-modification of a host copolymer block.[25,32-35] Otherwise, side-by-side interaction between nanorods leads to the formation of extended bundles that fill copolymer domains with perpendicularly aligned nanorods[25,29,30] or remain mutually disordered,[32,34] kinetically hinder microphase separation,[30,33,34] or just form a separate phase.[28,29,36] The authors of Ref. 34 have concluded that there exists a range of nanorod lengths optimal for their ordering in block copolymer domains. Shorter particles do not interact with copolymer blocks enough to be well-organized, whereas longer nanorods form clusters, which are believed to be kinetically trapped states.

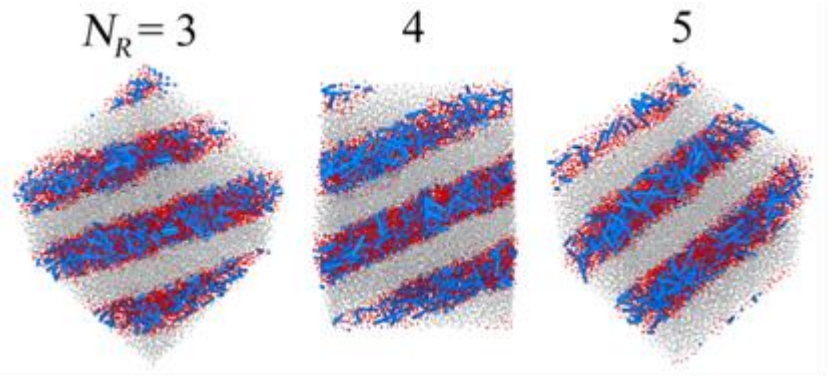

FIG. 5. Microphase-separated diblock copolymer $A_{10}B_{10}$ filled with highly selective ($\sigma = 1$) nanorods with $\phi_R = 0.1$ and $N_R = 3$, 4, and 5. Colors and repulsion parameters are the same as in Fig. 3.

Our study corroborates the experimental observations: nanorods with $N_R = 5$ are organized better than those with $N_R = 3$ (Figs. 5, 6), they do not reveal stacking even at high concentrations (Fig. 3), whereas longer ($N = 7$) nanorods with length close to the width of A domains demonstrate drastically different behavior shown in Fig. 7. At $\phi_R = 0.05$ they are mainly oriented along lamellae, but if their content is increased up to $\phi_R = 0.1$, the nanorods align across lamellae and stack side-by-side forming clusters that are inhomogeneously distributed in the A domains. Taking into account that clusters survive even after switching off the effective repulsion between A and B particles, such a behavior can

be considered as the macrophase separation of nanorods and the host block copolymer. At $\phi_R = 0.2$ long nanorods form their own lamellae aligned along block copolymer ones, in which individual nanorods are strictly perpendicular to the interface.

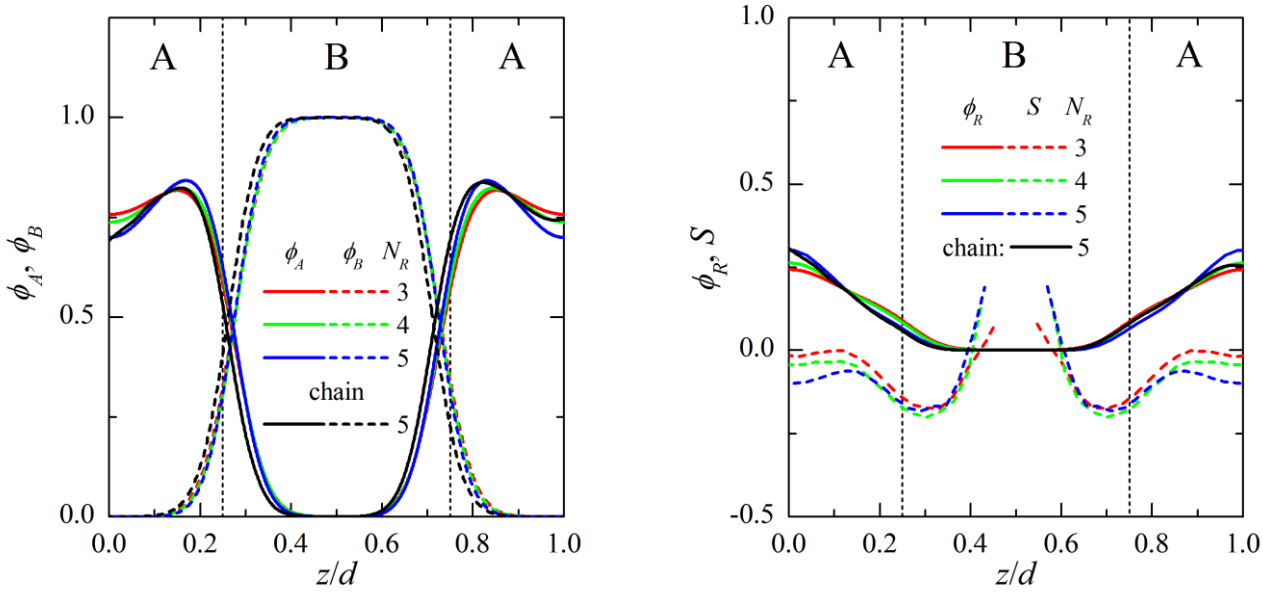

FIG. 6. The local volume fractions $\phi_A(z)$ and $\phi_B(z)$, of the A and B particles (left), the local fraction of the nanorods, $\phi_R(z)$, and the orientational order parameter, $S(z)$ (right), for different values of the nanorod length, N_R (specified), and for the flexible chains with $N_R = 5$. $\phi_R = 0.1$. Other parameters are as in Fig. 4.

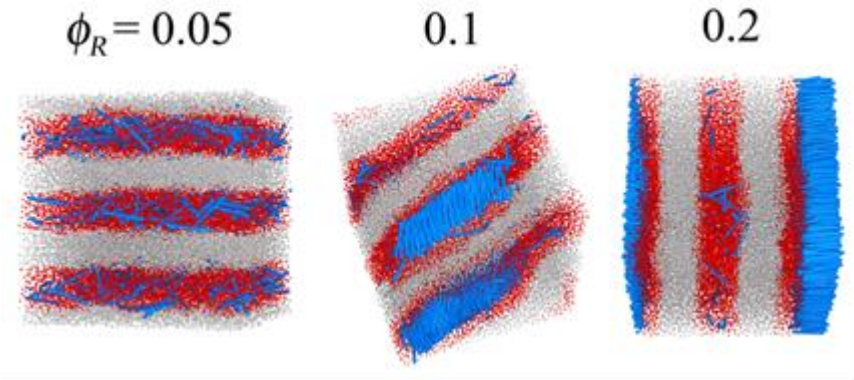

FIG. 7. Microphase-separated diblock copolymer $A_{10}B_{10}$ filled by highly selective ($\sigma = 1$) nanorods with $N_R = 7$ and $\phi_R = 0.05$, 0.1, and 0.2. Colors and repulsion parameters are as in Fig. 3.

Thus, both length and stiffness of the nanorods are the important factors that have to be optimized for designing anisotropic composites with macroscopically homogeneous structure.

D. Effect of the nanorod selectivity

In experiments the surface of nanoparticles can be modified to tune their interaction with a polymer matrix. So far we have considered nanorods highly selective towards one block of the diblock copolymer. An opposite case, when the nanorods are accumulated at the domain boundaries of a copolymer microstructure, is also quite possible. Migration of nanorods from A domains to the A/B interfaces is clearly visible in the snapshots of the stationary structures that correspond to different values of the selectivity parameter σ introduced before (Fig. 8). One can readily see that at the boundary the non-selective ($\sigma = 0$) nanorods are mainly aligned parallel to the lamellar plane, while in the A and B domains they tend to align in the perpendicular direction in order to reach the thermodynamically beneficial interface with their ends. This becomes even more clear after considering the distribution of the local parameters presented in Fig. 9.

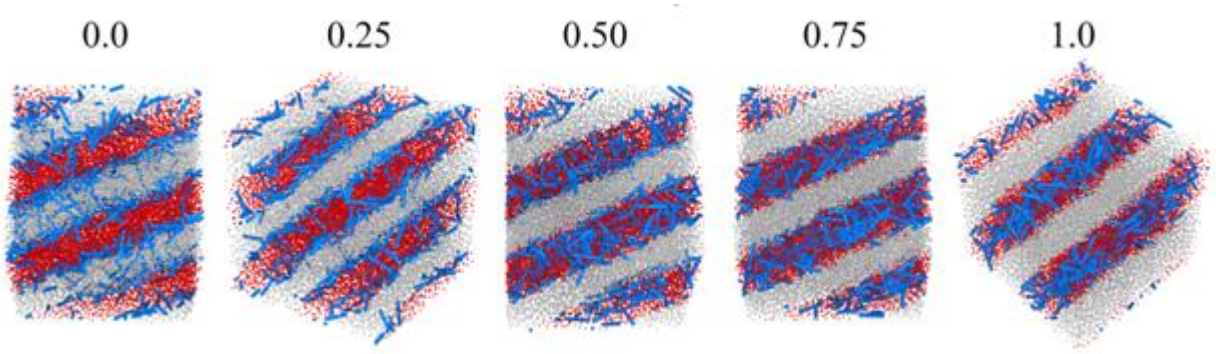

FIG. 8. Microphase-separated composites based on the diblock copolymer $A_{10}B_{10}$ (monomer units A and B are shown in red and grey, respectively) and nanorods (blue) with $\phi_R = 0.1$ and $N_R = 5$. The selectivity parameter σ is specified above each snapshot.

The less is the selectivity parameter, the more symmetrical are the distributions of A and B blocks and nanorods. Parallel (perpendicular) alignment of nanorods in A (B) domains is weakened, while their parallel orientation at the boundaries is only strengthened. At $\sigma = 0.5$ the maximum concentration of nanorods is achieved at the A/B interface. The nanorods are randomly distributed in the bulk of the A domains and are aligned mainly perpendicular to the boundary at the center of the B domains, although their concentration there is still very low. For $\sigma < 0.5$ the weak perpendicular alignment of nanorods ($S_{max} \approx 0.2$) is found in both A and B domains, while somewhat stronger ($S_{min} \approx -0.3$) tendency for the parallel alignment is found in the interfacial region.

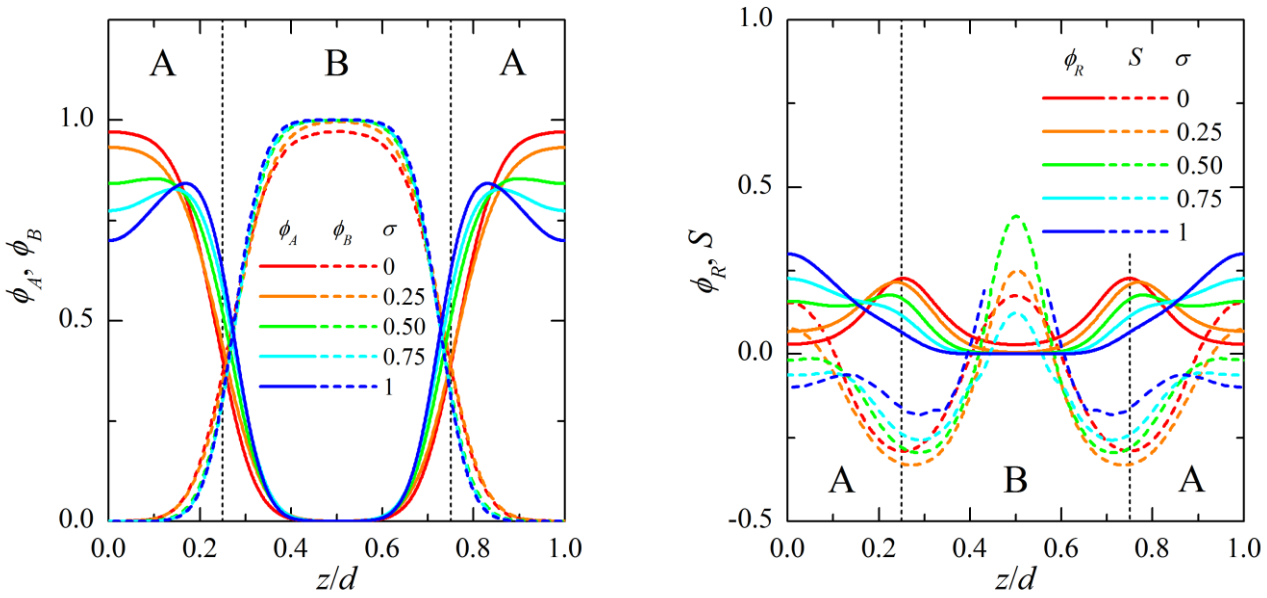

FIG. 9. The local volume fractions, $\phi_A(z)$ and $\phi_B(z)$, of the A and B particles (left), the local fraction of the nanorods, $\phi_R(z)$, and the orientational order parameter, $S(z)$ (right), for different values of the selectivity parameter σ (specified) with ϕ_R =0.1 and N_R = 5. Other details are as in Fig. 4.

It is interesting to compare the distribution and alignment of highly selective ($\sigma = 1$) and non-selective ($\sigma = 0$) nanorods. In both cases the most populous region (A domains and the A/B interfaces, respectively) is characterized by two to three times the fraction of nanorods as compared with the

average ϕ_R =0.1 and their preferential alignment parallel to the lamellae. However, this alignment effect is considerably more pronounced for the non-selective nanorods ($S_{min} \approx -0.3$) in comparison with the selective ones ($S_{min} \approx -0.1$). If nanorods are located predominantly in A domains, the latter swell that is seen from the shift of A/B boundaries in Fig. 9 from dashed vertical lines corresponding to the pure copolymer melt towards the center of the B domain. Non-selective nanorods are concentrated at the domain boundaries thus decreasing the number of A/B monomer unit contacts and, consequently, lowering the interfacial tension. At the same time their local concentration is still too low to interfere with A-B junctions of the diblock copolymer. Indeed, the total number of A-B junctions in our simulation cell is 41472 (number of DPD particles) × 0.9 (average copolymer fraction) / 20 (copolymer length) = 1866. Usually our cell hosts three A and B domains that means six A/B domain interfaces (Fig. 8). Taking r_c as the interfacial thickness and recalling that the cell thickness is 24 r_c, we find that 41472 × 0.9 × (6/24) = 9331 DPD particles are situated at the interface, where they form 9331/2 = 4665 contacts. This is a lower bound, since a particle can form several pairwise contacts and the interface can be thicker. Increasing the local concentration of nanorods at the interface from 0.1 to 0.2 means replacing 41472 × (0.2 – 0.1)×(6/24)/2 = 518 A/B contacts with A/R or B/R contacts. This seems to be a feasible task since at least 4665 – 1866 = 2799 A/B contacts (60%) at the interface are not junctions. Thus nanorod segregation to the domain boundaries should not considerably affect the lamella morphology of the composite.

To the best of our knowledge, composites with weakly- or non-selective interactions between polymer blocks and the nanorods have not been studied in laboratory experiments yet. Note that the affinity of spherical nanoparticles to copolymer blocks and therefore their preferential location can be effectively controlled by grafting suitable ligands to the particle surface.[73,74] Similar experimental studies with anisotropic nanoparticles would be highly desirable because in this particular case one expects the maximum difference in the degree of the orientational ordering of nanorods between the centers of the blocks and the boundaries of the lamellae. One also expects a non-zero local concentration of nanorods throughout the whole composite.

IV. COMPARISON WITH THE THEORY

In the general case the interaction between an anisotropic nanoparticle and an isotropic monomer unit of a polymer chain should be anisotropic, i.e., it should depend on the orientation of the unit vector $\boldsymbol{a}_i$ in the direction of the primary axis of the nanoparticle. In the case of a rod-like particle this unit vector is parallel to the symmetry axis of the rod. In the computer simulations of polymer nanocomposites, described above, the nanoparticle has been modeled by several isotropic interaction sites which directly interact with monomer units. One notes that the interaction between each site and the isotropic monomer unit is isotropic, but the sites are linked together in a rod-like structure, and as a result the total nanoparticle – monomer unit interaction potential becomes anisotropic, i.e., it depends on the orientation of the rod with respect to the intermolecular vector between the center of the nanoparticle and the monomer unit.

Multi-site model interaction potentials are common in computer simulations of anisotropic fluids, but they are generally too cumbersome to be used in a molecular-statistical theory. Instead we employ a simple interaction potential between the rod-like nanoparticle and the isotropic monomer units which is composed of the isotropic and anisotropic parts:

$$U(i,j) = J_{\mathrm{A}}(r_i - r_j) + I_{\mathrm{A}}(r_i - r_j)P_2(\boldsymbol{a}_i \cdot \mathbf{u}_{ij}) + J_{\mathrm{B}}(r_i - r_j) + I_{\mathrm{B}}(r_i - r_j)P_2(\boldsymbol{a}_i \cdot \mathbf{u}_{ij}), \qquad (4)$$

where $\mathbf{r}_i$ is the position vector of the nanoparticle i and $\boldsymbol{a}_i$ is the unit vector in the direction of its ~~the~~ long axis, $\mathbf{r}_{j\mathrm{A}}$ and $\mathbf{r}_{j\mathrm{B}}$ are the position vectors of the monomers A and B, respectively, $\mathbf{r}_{ij} = \mathbf{r}_i - \mathbf{r}_j$ and $\mathbf{u}_{ij}$ is the unit vector in the direction of $\mathbf{r}_{ij}$ and $P_2(\boldsymbol{a}\cdot\mathbf{u})$ is the second Legendre polynomial. Here J_{A}, J_{B} are the isotropic coupling constants between the nanoparticle and the monomers A and B, respectively, while I_{A}, I_{B} are the corresponding anisotropic interaction constants. The anisotropic interaction between isotropic monomers and anisotropic nanoparticles in Eq. (4) describes the coupling between the long axis of a nanoparticle $\boldsymbol{a}_i$ and the unit vector $\mathbf{u}_{ij}$ pointing from the particle to the monomer.

In the molecular field approximation the single particle density distribution function, which depends on nanoparticle positions and orientations, can be expressed in the form of the Boltzmann distribution:

$$f(\boldsymbol{a}_i, \mathbf{r}_i) = \frac{1}{Z} \exp\left[-\frac{U_{MF}(\boldsymbol{a}_i, \mathbf{r}_i)}{k_B T} \right] \tag{5}$$

where Z is the normalization factor (partition function) and the mean-field potential is obtained by averaging the interaction potential of Eq. (4) over all positions of monomers A and B in the microphase-separated state:

$$\begin{aligned} U_{MF}(\boldsymbol{a}, \mathbf{r}) = & \int \left[J_{\mathrm{A}}(\mathbf{r} - \mathbf{r}') + I_{\mathrm{A}}(\mathbf{r} - \mathbf{r}') P_2(\boldsymbol{a} \cdot \mathbf{u}) \rho_{\mathrm{A}}(\mathbf{r}') d^3\mathbf{r}' \right] \\ & + \int \left[(J_{\mathrm{B}}(\mathbf{r} - \mathbf{r}') + I_{\mathrm{B}}(\mathbf{r} - \mathbf{r}') P_2(\boldsymbol{a} \cdot \mathbf{u})) \rho_{\mathrm{B}}(\mathbf{r}') d^3\mathbf{r}' \right] \end{aligned} \tag{6}$$

where ρ_{A}, ρ_{B} are the local densities of monomers A and B, respectively.

Using the distribution function of Eq. (5), the local orientational order parameter of anisotropic nanoparticles can be written in the form:

$$S(\mathbf{r}) = \left\langle P_2(\boldsymbol{a}_i \cdot \mathbf{k}) \right\rangle = \frac{\int P_2(\boldsymbol{a}_i \cdot \mathbf{k}) f(\boldsymbol{a}_i, \mathbf{r}) d^2\boldsymbol{a}_i}{\int f(\boldsymbol{a}_i, \mathbf{r}) d^2\boldsymbol{a}_i}, \tag{7}$$

where **k** is the block interface normal vector.

As shown in Ref. 46, in the limiting case of strong (or, more precisely, superstrong,[75] when domain boundaries are of the order of the monomer unit size) segregation it is possible to obtain an explicit analytical expression for the mean-field potential assuming for simplicity that $J_\alpha(\mathrm{r}) = J_{0\alpha} r^{-6}$ and $I_\alpha(\mathrm{r}) = I_{0\alpha} r^{-6}$ and, where α = A, B.

For $z > R_0$ where the z-axis is perpendicular to the flat boundary between the blocks, R_0 is the radius of nanoparticle-monomer unit interaction and $z = 0$ at the boundary:

$$U_{MF}^{(0)}(\boldsymbol{a}, z) = -\int_{r_0}^{R_0} r^{-4} dr \int_0^1 d\cos\theta \int_0^{2\pi} d\phi \left[\Delta J + \Delta I P_2(\boldsymbol{a} \cdot \mathbf{u}) \right] = \frac{2\pi}{3} \Delta J (R_0^{-3} - r_0^{-3}) \tag{8}$$

For $r_0 < z < R_0$, where r_0 is the nanoparticle radius:

$$U_{MF}^{(1)}(\boldsymbol{a},z)=-\left[\int_{r_0}^{z}dr\int_0^1 d\cos\theta+\int_z^{R_0}dr\int_0^{z/r}d\cos\theta\right]2\pi r^{-4}\left[\Delta J+\Delta IP_2(\cos\theta)P_2(\mathbf{k}\cdot\boldsymbol{a})\right]$$
$$=\frac{2\pi}{3}\Delta J(z^{-3}-r_0^{-3})+\frac{\pi z}{2}(\Delta J-\Delta IP_2(\mathbf{k}\cdot\boldsymbol{a})/2)(R_0^{-4}-z^{-4})+\frac{\pi z^3}{6}\Delta IP_2(\mathbf{k}\cdot\boldsymbol{a})(R_0^{-6}-z^{-6}) \quad (9)$$

For z < r_0:

$$U_{MF}^{(2)}(\boldsymbol{a},z)=-\int_{r_0}^{R_0}dr\int_0^{z/r}d\cos\theta\,2\pi r^{-4}\left[\Delta J+\Delta IP_2(\cos\theta)P_2(\mathbf{k}\cdot\boldsymbol{a})\right]$$
$$=\frac{\pi z}{2}(\Delta J-\Delta IP_2(\mathbf{k}\cdot\boldsymbol{a})/2)(R_0^{-4}-r_0^{-4})+\frac{\pi z^3}{6}\Delta IP_2(\mathbf{k}\cdot\boldsymbol{a})(R_0^{-6}-r_0^{-6}) \quad (10)$$

Here $\Delta J(\mathrm{r}) = J_{0\mathrm{A}} - J_{0\mathrm{B}}$ and $\Delta I(\mathrm{r}) = I_{0\mathrm{A}} - I_{0\mathrm{B}}$.

One notes that in the middle of the block the mean-field potential is constant, i.e., it depends neither on the nanoparticle position nor on its orientation because the surrounding medium is isotropic and homogeneous. In contrast, in the boundary region the mean-field potential depends on the distance between the nanoparticle and the boundary between domains and on the orientation of the nanoparticle axis. In this region a nanoparticle interacts simultaneously with monomer units of both kinds, located in domains A and B, and as a result the average interaction becomes anisotropic. Note also that for the particle close to the domain boundary, the mean-field potential is an odd function of *z* and it vanishes when the particle center is directly at the boundary.

In the case of weak segregation the difference between the local densities of monomer units A and B is relatively small and in the first approximation it can be expressed as $\rho(\mathbf{r}_1) - \rho(\mathbf{r}_2) = \delta\cos(\mathbf{q}\cdot\mathbf{r_{12}})$ where **q** is the wave vector of the microphase structure and δ is the corresponding amplitude. In this case the mean-field potential is given by the following expression[46]

$$U_{MF}(\boldsymbol{a},\mathbf{r})=\delta\cos(\mathbf{q}\cdot\mathbf{r})\left[\Delta J_q+\Delta I_q P_2(\boldsymbol{a}\cdot\mathbf{k})\right], \quad (11)$$

where

$\Delta J_q = 2\pi\int r^2 dr\int d\cos\theta\,\Delta J(r)\cos(qr\cos\theta)$ and $\Delta I_q = 2\pi\int r^2 dr\Delta I(r)\int d\cos\theta\,P_2(\cos\theta)\cos(qr\cos\theta)$.

The density and orientational order parameter profiles in the lamellae phase have been calculated numerically in the limiting cases of strong and weak segregation, and the characteristic results are presented in Fig. 10. One can readily see that the results of the molecular theory are qualitatively similar

to those obtained by computer simulations even though there are significant quantitative discrepancies. In particular, in the framework of this simple theoretical model the anisotropic nanoparticles are orientationally ordered in a boundary region between the blocks due to the selectivity of the interaction between the particle and the monomer units of the two different kinds which is described by the constants ΔJ and ΔI. Similar to the results of computer simulations, the orientational (nematic) order parameter possesses opposite signs in different blocks, that is the long axes of anisotropic nanoparticles are aligned parallel to the boundary between the blocks on one side of the boundary and perpendicular to the boundary on another side. As expected, the nanoparticles are mostly located in the block with the strongest isotropic interaction between the monomer units and the nanoparticles.

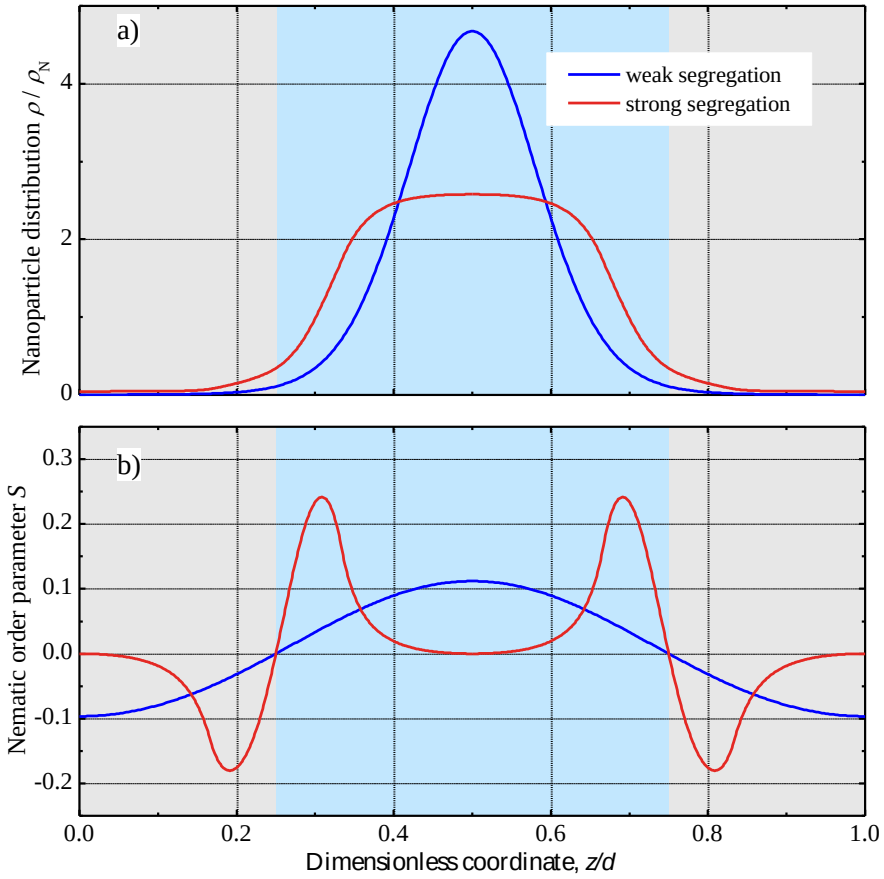

FIG. 10. (a) The theoretical local volume fraction, $\phi_R(z)$, and (b) orientational order parameter, $S(z)$, of nanoparticles across the lamellar diblock copolymer domains A (grey) and B (light blue) in the case of strong (red curves) and weak (blue) segregation. The domains thickness is $d = 2d_A = 2d_B =$

$12r_0$, the interaction radius $R_0 = 3r_0$, the isotropic and anisotropic interaction constants are $\Delta J = k_BT$, $\Delta J_q = 3.72\Delta J$ and $\Delta I = -3k_BT$, $\Delta I_q = -0.175\Delta I$, respectively.

In the framework of this simple theoretical model the anisotropic nanoparticles are orientationally ordered only in the boundary region while in the computer simulations they are also ordered inside the domains. This is mainly related to the difference in model interaction potentials. In the theoretical model monomer units interact with the center of a nanoparticle while in computer simulations the corresponding interaction centers are distributed along the nanorod with the length comparable with the size of a block. As a result the center of such a nanorod may be located in the central part of the block and the ends may be located close to the boundary depending on its orientation. The effective anisotropy of the total interaction potential is then determined by the interaction of the ends with the monomer units of the adjacent block.

One can readily see that qualitatively the orientational order parameter profiles obtained by computer simulations are somewhat between the theoretical profiles obtained in the limits of strong (in fact superstrong that corresponds to an infinitely thin domain boundary) and weak segregation. This is partially explained by the fact that in the computer simulations the segregation is strong but not ideal. Another reason for a broader nanoparticle distribution in the simulations lies in the local averaging of *z*-coordinates and orientations of all segments connecting DPD particles within nanorods, whereas the theory identifies *z*-coordinates of anisotropic nanoparticles with their centers.

V. CONCLUSION AND OUTLOOK

In this paper a model composite consisting of a diblock copolymer and anisotropic nanoparticles (nanorods) was considered. As far as we are aware, for the first time the main focus was laid on the local distribution and orientation order of nanorods in the lamellar microstructure formed by immiscible copolymer blocks. The role of nanorod content, length, stiffness, and selectivity has been studied. Similar to the experimental data, selective location of nanorods in one of the copolymer domains and

their orientation along the axis of the lamellae structure are the most common effects. The host diblock copolymer matrix keeps its lamellar structure for all values of the nanorod volume fraction. When the volume fraction of short nanoparticles exceeds 0.1, the domain defects become visible, whereas long nanorods can form their own phase, in which they are stacked side by side. Thus we do not support the prediction of Ref. 48 concerning the possible transformation of a lamellar morphology into the hexagonal one with the increasing nanorod concentration, which has been found in simulations using a much smaller box.

An interesting result is the possibility of mutually perpendicular alignment of nanoparticles in the adjacent domains, which follows both from the coarse-grained molecular dynamics (DPD) simulation of nanorods and from the molecular theory which takes into consideration the anisotropic interaction between anisotropic nanoparticles of the spherical shape and the monomer units. Experimental verification of this prediction can be complicated, however, as the nanorod alignment perpendicular to the block boundaries in the lamellae phase is strongly correlated with a decrease in their local concentration. It seems that the most promising system in which the predicted alignment effect may be observed is a composite with non-selective nanoparticles. In this case, which corresponds to the leftmost snapshot in Fig. 8, the majority of the nanorods are located close to the domain boundaries and align along them, while a small but non-vanishing fraction of the nanorods reside inside domains and are aligned in the perpendicular direction.

The present simulations can be extended to include asymmetric copolymers forming cylindrical micelles as a step towards the detailed study of the phase diagram of diblock copolymer – nanorods composites. From the theoretical standpoint, it would be interesting to consider non-spherical nanoparticles like dumbbells in order to investigate the correspondence between shape anisometry and anisotropy of the interaction potential.

ACKNOWLEDGEMENT The authors are grateful to the Russian Science Foundation (Project 16-13-10280) for financial support and to the Moscow State University Supercomputer Center for the access to the supercomputer “Lomonosov”.

REFERENCES

1. C.M. Bates and F.S. Bates, Macromolecules **50**, 3 (2017).
2. M. Luo and T.H. Epps, III, Macromolecules **46**, 7567 (2013).
3. H. Hu, M. Gopinadhan and C.O. Osuji, Soft Matter **10**, 3867 (2014).
4. C.M. Bates, M.J. Maher, D.W. Janes, C.J. Ellison and C.G. Willson, Macromolecules **47**, 2 (2014).
5. P.D. Topham, A.J. Parnell and R.C. Hiorns, J. Polym. Sci. Part B: Polym. Phys. **49**, 1131 (2011).
6. V. Abetz, Macromol. Rapid Commun. **36**, 10 (2015).
7. F.S. Bates, M.A. Hillmyer, T.P. Lodge, C.M. Bates, K.T. Delaney and G.H. Fredrickson, Science **336**, 434 (2012).
8. M.R. Bockstaller, R.A. Mickiewicz, E.L. Thomas, Adv Mater. **17**, 1331 (2005).
9. T.N. Hoheisel, K. Hur and U.B. Wiesner, Prog. Polym. Sci. **40**, 3 (2015).
10. S. Biswajit and P. Alexandridis, Prog. Polym. Sci. **40**, 33 (2015).
11. M.A. Boles, M. Engel and D.V. Talapin, Chem. Rev. **116**, 11220 (2016).
12. A.C. Balazs, T. Emrick and T.P. Russell, Science **314**, 1107 (2006).
13. V.A. Gerasin, E.M. Antipov, V.V. Karbushev, V.G. Kulichikhin, G.P. Karpacheva, R.V. Talroze and Y.V. Kudryavtsev, Russ. Chem. Rev. **82**, 303 (2013).
14. C. Liedel, K.A. Schindler, M.J. Pavan, C. Levin, C.W. Pester, M. Ruppel, V.S. Urban, R. Shenhar and A. Böker, Small **19**, 3276 (2013).
15. S. Samant, S.T. Hailu, A.M. Al-Enizi, A. Karim and D. Raghavan, J. Polym. Sci. Part B: Polym. Phys. **53**, 604 (2015).
16. R. M. Mutiso and K. I. Winey, Prog. Polym. Sci. **40**, 63 (2015).

17. J. Albuerne, A. Boschetti-de-Fierro, C. Abetz, D. Fierro and V. Abetz, Adv. Eng. Mater. **13**, 803 (2011).

18. A.-C. Baudouin, J. Devaux and C. Bailly, Polymer **51**, 1341 (2010).

19. A.-C. Baudouin, D. Auhl, F. Tao, J. Devaux and C. Bailly, Polymer **52**, 149 (2011).

20. A. Göldel and P. Pötschke, In: Polymer Carbon Nanotube Composites : Preparation, Properties and Applications; McNally T.; Pötschke P., Eds. (Woodhead, New Delhi, 2011), Chapter 19, 587-620.

21. B. Du, U. A. Handge, M. Wambach, C. Abetz, S. Rangou and V. Abetz, Polymer **54**, 6165 (2013).

22. Handbook of Nanophysics: Nanoparticles and Quantum Dots, Sattler K.D, Ed. (CRC Press, Boca Raton, 2011)

23. Complex-shaped Metal Nanoparticles: Bottom-up Syntheses and Applications, Sau T.K. and Rogach A.L., Eds. (Wiley-VCH, Weinheim, 2012).

24. R. D. Deshmukh, Y. Liu and R. J. Composto, Nano Lett. **7**, 3662 (2007).

25. W. Li, P. Zhang, M. Dai, J. Hie, T. Babu, Y.-L. Xu, R. Deng, R. Liang, M.-H. Lu, Z. Nie and J. Zhu, Macromolecules **46**, 2241 (2013).

26. B. Rasin, H. Chao, G. Jiang, D. Wang, R. A. Riggleman and R. J. Composto, Soft Matter **12**, 2177 (2016).

27. J. G. Son, W. K. Bae, H. Kang, P. F. Nealey and K. Char, ACS Nano **3**, 3927 (2009).

28. Q. L. Zhang, S. Gupta, T. Emrick and T. P. Russell, J. Am. Chem. Soc. **128**, 3898 (2006).

29. E. Ploshnik, A. Salant, U. Banin and R. Shenhar, Adv. Mater. **22**, 2774 (2010).

30. E. Ploshnik, A. Salant, U. Banin and R. Shenhar, Phys. Chem. Chem. Phys. **12**, 11885 (2010).

31. A. Halevi, S. Halvini, M. Oded, A.H. E. Müller, U. Banin and R. Shenhar, Macromolecules **47**, 3022 (2014).

32. K. Thorkelsson, A. J. Mastroianni, P. Ercius and T. Hu, Nano Lett. **12**, 498 (2012).

33. K. Thorkelsson, J. H. Nelson, A. P. Alivisatos and T. Hu, Nano Lett. **13**, 4908 (2013).

34. K. Thorkelsson, N. Bronstein and T. Hu, Macromolecules **49**, 6669 (2016).

35. K. H. Ku, H. Yang, J. N. Shin and B. J. Kim, J. Polym. Sci. Part A: Polym. Chem. **53**, 188 (2015).

36. C.-T. Lo, M.-H. Li and W.-T. Lin, J. Chem. Phys. **142**, 184903 (2015).

37. G. H. Fredrickson, V. Ganesan and F. Drolet, Macromolecules **35**, 16 (2002).

38. M. W. Matsen, J. Phys.: Condens. Matter **14**, R21 (2002).

39. Z. Shou, G. A. Buxton, and A. C. Balazs, Compos. Interfaces **10**, 343 (2003).

40. K. Hur, R. G. Hennig, F. A. Escobedo, and U. Wiesner, J. Chem. Phys. **133**, 194108 (2010).

41. S. Sides, B. Kim, E. Kramer, and G. Fredrickson, Phys. Rev. Lett. **96**, 250601 (2006).

42. J. U. Kim and M. W. Matsen, Phys. Rev. Lett. **102**, 078303 (2009).

43. H. Chao, B. A. Hagberg and R. A. Riggleman, Soft Matter **10**, 8083 (2014).

44. J. Koski, H. Chao and R. A. Riggleman, J. Chem. Phys. **139**, 244911 (2013).

45. Q.-Y. Tang and Y.-Q. Ma, J. Phys. Chem. B **113**, 10117 (2009).

46. M. A. Osipov and M. V. Gorkunov, Eur. Phys. J. E **39**, 126 (2016).

47. L.-T. Yan and X.-M. Xie, Prog. Polym. Sci. **38**, 369 (2013).

48. L. He, L. Zhang, A. Xia and H. Liang, J. Chem. Phys. **130**, 144907 (2009).

49. L. He, L. Zhang, H. Chen and H. Liang, Polymer **50**, 3403 (2009).

50. L. He, L. Zhang and H. Liang, Polymer **51**, 3303 (2010).

51. A. Chai, D. Zhang, Y. Jiang, L. He and L. Zhang, J. Chem. Phys. **139**, 104901 (2013).

52. Z. Zhang, T. Li and E. Nies, Macromolecules **47**, 5416 (2014).

53. P. J. Hoogerbrugge and J. M. V. A. Koelman, Europhys. Lett. **19**, 155 (1992).

54. J. M. V. A. Koelman and P. J. Hoogerbrugge, Europhys. Lett. **21**, 363 (1993).

55. P. Espanol and P. B. Warren, Europhys. Lett. **30**, 191 (1995).

56. R. D. Groot and P. B. Warren, J. Chem. Phys. **107**, 4423 (1997).

57. T. F. Miller, M. Eleftheriou, P. Pattnaik, A. Ndirango, D. Newns and G. J. Martyna, J. Chem. Phys. **116**, 8649 (2002).

58. Y. K. Levine, A. E. Gomes, A. F. Martins and A. Polimeno, J. Chem. Phys. **122**, 144902 (2005).

59. Z. Zhang and H. Guo, J. Chem. Phys. **133**, 144911 (2010).

60. http://lammps.sandia.gov/

61. G. Besold, I. Vattulainen, M. Karttunen and J. M. Polson, Phys. Rev. E **62**, R7611 (2000).

62. A. AlSunaidi, W. K. den Otter and J. H. R. Clarke, Phil. Trans. R. Soc. Lond A 362, 1773 (2004).

63. A. Polimeno, A. Gomes and A. F. Martins, In: Computer Simulation of Liquid Crystals and Polymers, NATO Science Series II: Mathematics, Physics and Chemistry, V. 177; Pasini P., Zannoni C., Žumer S., Eds. (Kluwer, Dordrecht, 2005).

64. A. A. Gavrilov, Y. V. Kudryavtsev, P. G. Khalatur and A. V. Chertovich, Chem. Phys. Lett. **503**, 277 (2011).

65. L. Leibler, Macromolecules **13**, 1602 (1980).

66. G. H. Fredrickson and E. Helfand, J. Chem. Phys. **87**, 697 (1987).

67. R. D. Groot and T. J. Madden, J. Chem. Phys. **108**, 8713 (1998).

68. A. A. Gavrilov, Y. V. Kudryavtsev and A. V. Chertovich, J. Chem. Phys. **139**, 224901 (2013).

69. O. N. Vassiliev and M. W. Matsen, J. Chem. Phys. **118**, 7700 (2003).

70. J. Glaser, P. Medapuram, T. M. Beardsley, M. W. Matsen and D. C. Morse, Phys. Rev. Lett. **113**, 068302 (2014).

71. P. Medapuram, J. Glaser and D. C. Morse, Macromolecules **48**, 819 (2015).

72. T. Beardsley and M. W. Matsen, Phys. Rev. Lett. **117**, 217801 (2016).

73. B. J. Kim, J. Bang, C. J. Hawker and E. J. Kramer, Macromolecules **39**, 4108 (2006).

74. T. Nakano, D. Kawaguchi and Y. Matsushita, JACS **135**, 6798 (2013).

75. I. A. Nyrkova, A. R. Khokhlov and M. Doi, Macromolecules **26**, 3601 (1993).